JBC RESEARCH ARTICLE

Sdr16c5 and *Sdr16c6* control a dormant pathway at a bifurcation point between meibogenesis and sebogenesis

Received for publication, February 21, 2023, and in revised form, March 23, 2023 Published, Papers in Press, April 17, 2023,
https://doi.org/10.1016/j.jbc.2023.104725

Igor A. Butovich[1,2,*], Amber Wilkerson[1], Kelli R. Goggans[3], Olga V. Belyaeva[3], Natalia Y. Kedishvili[3], and Seher Yuksel[1]

From the [1]Department of Ophthalmology, and [2]Graduate School of Biomedical Sciences, University of Texas Southwestern Medical Center, Dallas, Texas, USA; [3]Department of Biochemistry and Molecular Genetics, Heersink School of Medicine, University of Alabama at Birmingham, Birmingham, Alabama, USA

Reviewed by members of the JBC Editorial Board. Edited by Qi-Qun Tang

Genes *Sdr16c5* and *Sdr16c6* encode proteins that belong to a superfamily of short-chain dehydrogenases/reductases (SDR16C5 and SDR16C6). Simultaneous inactivation of these genes in double-KO (DKO) mice was previously shown to result in a marked enlargement of the mouse Meibomian glands (MGs) and sebaceous glands, respectively. However, the exact roles of SDRs in physiology and biochemistry of MGs and sebaceous glands have not been established yet. Therefore, we characterized, for the first time, meibum and sebum of *Sdr16c5/Sdr16c6*-null (DKO) mice using high-resolution MS and LC. In this study, we demonstrated that the mutation upregulated the overall production of MG secretions (also known as meibogenesis) and noticeably altered their lipidomic profile, but had a more subtle effect on sebogenesis. The major changes in meibum of DKO mice included abnormal accumulation of shorter chain, sebaceous-type cholesteryl esters and wax esters (WEs), and a marked increase in the biosynthesis of monounsaturated and diunsaturated Meibomian-type WEs. Importantly, the MGs of DKO mice maintained their ability to produce typical extremely long chain Meibomian-type lipids at seemingly normal levels. These observations indicated preferential activation of a previously dormant biosynthetic pathway that produce shorter chain, and more unsaturated, sebaceous-type WEs in the MGs of DKO mice, without altering the elongation patterns of their extremely long chain Meibomian-type counterparts. We conclude that the *Sdr16c5/Sdr16c6* pair may control a point of bifurcation in one of the meibogenesis subpathways at which biosynthesis of lipids can be redirected toward either abnormal sebaceous-type lipidome or normal Meibomian-type lipidome in WT mice.

Exocrine Meibomian glands (MGs) (1) are essential components of the ocular defense system that protects the eye from desiccation by providing their holocrine lipid-rich secretion called meibum (2, 3). MGs are embedded into tarsal plates (TPs) of the eyelids and continuously produce and excrete meibum *via* a ductal system directly onto the ocular surface (4–6). Then, meibum mixes with other secretions that are produced by lacrimal glands, goblet cells in the conjunctiva, and some other parts of the ocular surface and adnexa and forms a complex and dynamic structure called the tear film (7–10). Intricate interactions between components of these secretions determine, in a large measure, stability of the tear film, and, in the end, its ability to protect the eye (11). Both the amount of meibum that is produced by MGs and its quality (*i.e.*, chemical composition) are essential for the health of the eye (12, 13). Importantly, widespread ocular pathologies, such as MG dysfunction and Dry Eye (especially its evaporative form) were linked to either insufficient meibum production/delivery or abnormal lipid composition (13).

Previous studies highlighted the roles of a group of specific genes and enzymes that are involved in the biosynthesis of meibum (termed meibogenesis (3, 14)), which includes elongases of very long-chain fatty acids (ELOVLs) (15–18)], fatty acid desaturases (*e.g.*, SCD1) (19), fatty acid reductases (FARs) (20, 21), wax ester (WE) synthases (AWATs) (22–24)], cholesteryl ester (CE) synthases (SOATs) (25, 26), cytochrome P450 CYP4F39 (27) and a range of other genes and enzymes that are responsible for various steps of meibogenesis (3, 14, 26). Importantly, lipids of meibum are vastly different from those of other tissues and secretions, including a related secretion sebum (28). Thus, the molecular mechanisms of meibogenesis are likely to be different from lipid metabolism in other organs and tissues and are currently a subject of active research in various laboratories throughout the world.

However, it remains essentially unknown how this complex system of convoluted biosynthetic reactions is regulated *in vivo*. Recent reports on the role of peroxisome proliferator-activated receptor gamma (29, 30), omega-3 fatty acids (30, 31), and rosiglitazone (32) have not provided any evidence of stimulation or inhibition of meibogenesis per se in tested cells or animals, though stimulation of trivial lipogenesis that is characterized by an increase in biosynthesis of phospholipids and triacylglycerols (TAGs), was likely.

Importantly, in a recent report by Wu *et al.* (33), double inactivation of two related genes *Sdr16c5* and *Sdr16c6* was demonstrated to cause considerable enlargement of MGs, eyelid dysmorphism, and accelerated hair growth in mice. Characteristically, single mutation in the *Sdr16c6* gene did not cause any changes in the ocular phenotype, which was

* For correspondence: Igor A. Butovich, igor.butovich@utsouthwestern.edu.

explained as a possible functional redundancy of the genes. Abnormalities in the ocular phenotype reported by Wu *et al.* were similar to those that were reported for various mouse gene KO models that targeted critical genes of meibogenesis, such as *Elovl4, Elovl3, Elovl1, Awat2, Soat1, Cyp4f39, Far1/Far2,* and *Scd1*, and included a slit-eye phenotype and puffed eyelids, among other abnormalities. The effects of *Sdr16c5* and *Sdr16c6* inactivating mutations were proposed to be linked to the retinol-signaling pathway that was impacted in double KO (DKO) mice, but no changes in meibogenesis have been evaluated quantitatively or qualitatively.

Thus, the goal of this study was to characterize the effects of simultaneous inactivation of *Sdr16c5* and *Sdr16c6* on meibogenesis in mice, to determine what parts of it might be controlled by these genes, and explore whether this condition can be related to human MG pathologies. Since Meibomian lipids (MLs) are comprised of several hundred different species, in this paper we focused only on major components of meibum (such as WEs, CEs, TAGs, and cholesterol), leaving other lipid classes for future studies that will be conducted by this and/or other laboratories.

Results

Unsupervised and supervised multivariate statistical analyses of MLs from WT and double KO mice

The samples of extracted lipids were subjected to a gradient reverse phase ultra high performance chromatographic—high-resolution Time-of-Flight mass-spectrometric analyses (UPLC—MS^E). For detecting major lipid metabolites, the MS experiments were conducted using atmospheric pressure chemical ionization (APCI) in the positive ion mode (PIM). Typical total ion chromatograms (TICs; shown in Fig. 1, *A* and *B*) implied the existence of large differences between the two types of samples. Importantly, the multiple injections of the same sample and TICs of four WT samples were virtually indistinguishable from one another and so were TICs of eight DKO samples (Fig. S1).

When the MS spectra of the samples obtained between 5 and 50 min of the UPLC run were combined, the resulting observation mass spectra of WT and DKO samples produced very different patterns (Fig. 1, *C* and *D*). To determine MS signals which differed most significantly and reproducibly between two types of meibum in an unbiased fashion, the raw data obtained for four WT mice and eight homozygous DKO mice were imported in the Progenesis QI software (Waters Corp) and processed using its built-in algorithms. About 1012 variables, *i.e.*, analytes with unique combinations of UPLC retention times and *m/z* values (Table S1), were identified in each of the 12 samples. The entire 12 × 1012 dataset was exported to EZinfo for further processing using Principal Component Analysis (PCA) approaches, such as its unsupervised PCA-X and a supervised Orthogonal Projections to Latent Structures Discriminant Analysis (OPLS-DA) built-in models. The PCA-X model used Pareto scaling with no transformations. The R2X(Cum), *i.e.*, the variance explained, was 97% for two components with a high prediction power. The study samples produced two clearly separated, but tight, groups (Fig. 2*A*). The intragroup variability of the samples [*i.e.*, dispersion of samples along the $t(2)$ axis on the graph] was much lower than their intergroup differences [*i.e.*, dispersion along the $t(1)$ axis], with just one WT sample barely reaching, but not exceeding, the Hotelling's T2 95% confidence ellipse. Note that the same sample had somewhat higher levels of compounds eluting between 12 and 20 min into the run (labeled with asterisks in Fig. S1). The Goodness-of-Fit plot (≈0.98) demonstrated that the experimental observations and a fitted model were in a good agreement, while a Loadings Bi–Plot (Fig. 2*B*) revealed a wide range of variables that were associated with either WT or DKO specimens. The PCA-X analysis identified two major sample clusters in specimens, with just one WT sample bordering (but not crossing) the 95% confidence threshold. Therefore, no study samples were excluded from further analyses.

However, the unsupervised PCA-X model does not address the question of which variables have the strongest, statistically significant effect on the separation of the two types of the samples. Therefore, the data were reanalyzed in EZinfo using its supervised OPLS-DA modeling tool. The OPLS-DA analysis of WT and DKO samples was conducted using the same Pareto scaling with no transformation, which resulted in a model with R2Y(Cum) (variance explained) and a Q2(Cum) (variance predicted) of 99% each. On the Loadings Bi-Plot plot (Fig. 2*C*), the samples grouped similarly to the PCA-X groups shown in Figure 2, *A* and *B*. An excellent fit and predicting power of the model was evident from the Goodness-of-Fit plot (≈1), while the Distance-to-Model plot demonstrated that all but one DKO sample fell below the D-Crit (95%) level with no atypical samples observed (Fig. S2). A group of 40 variables with the highest influence on the separation of WT and DKO samples was identified from the variable importance plot (Fig. 2*D*). Note a rather low variability, *i.e.*, high statistical reliability, of the observations.

However, variable importance plots do not provide information on the directions (up or down) in which variables change in the study groups of samples and merely rank them according to their influence on the separation between the groups. Therefore, the data were transformed and displayed as an S-Plot (Fig. 2*E*). The S-Plot made it possible to identify the most influential variables which were increased or decreased in the groups of samples and evaluate the statistical significance of the changes in any particular variable among 1012 variables identified in the samples. The more distant the variables are from the origin of the *X*-axis ($X = 0$), the more they differ between the samples, and the farther they are from the origin of the *Y*-axis ($Y = 0$), the more statistically significant the differences are. In Figure 2*E*, the lower left quadrant displays the variables that are specific to DKO samples, while the upper right quadrant contains variables that are characteristic of WT samples. Due to the large number of variables, only a few of them are labeled in the graph. However, this analysis allowed for compiling a starting list of analytes for *targeted* analyses of WT and DKO Meibomian lipidomes, which are discussed below.

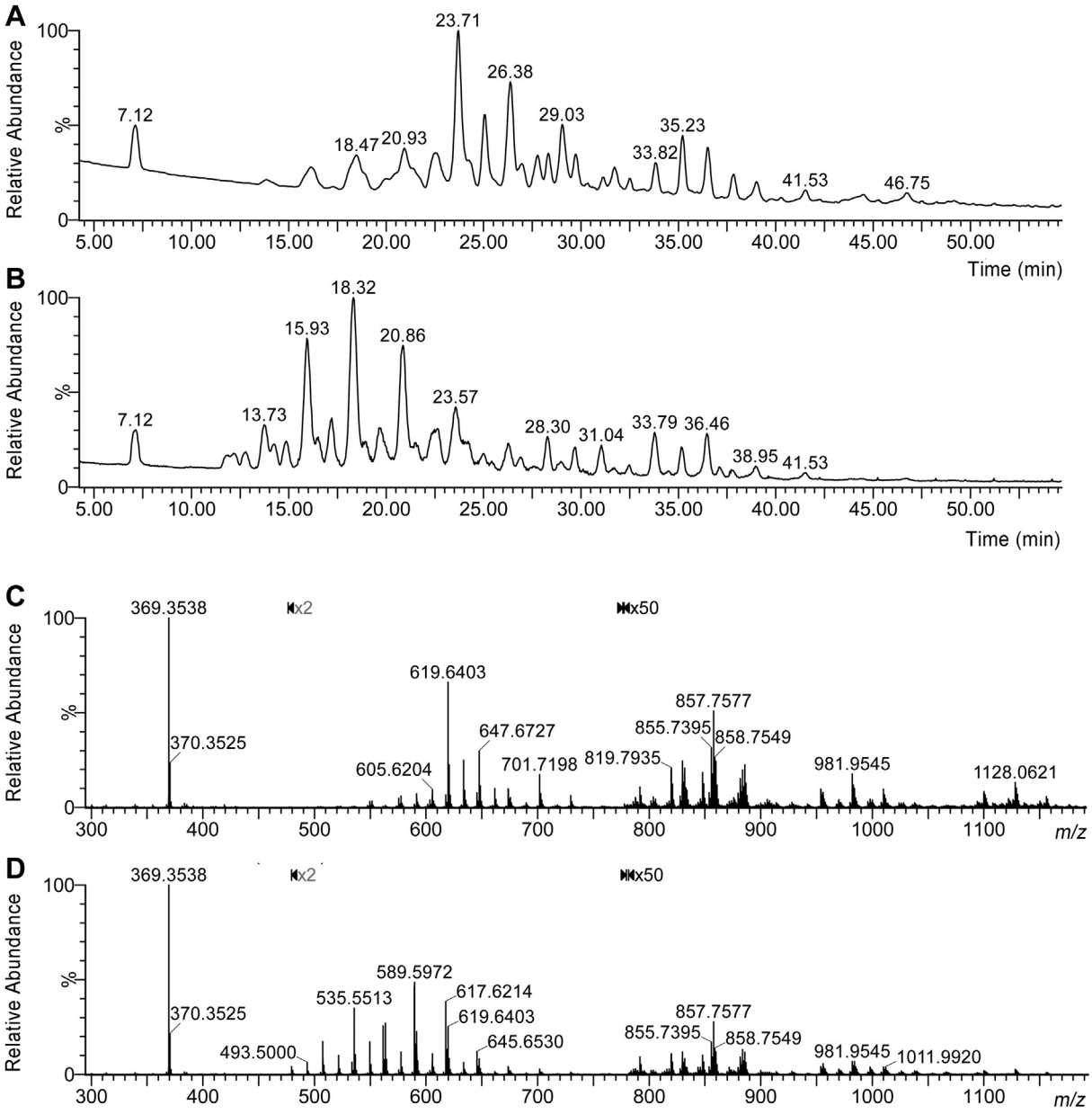

Figure 1. Total ion chromatograms (TIC) and observation mass spectra of WT and double KO (DKO) mouse tarsal plate extracts. *Panel A*, a TIC of a representative WT sample obtained in atmospheric pressure chemical ionization positive ion mode using reverse phase chromatography on a C_{18} BEH Acquity column. *Panel B*, a TIC of a representative DKO sample obtained in the same experimental conditions. *Panel C*, an observation mass spectrum of the WT sample shown in Panel A obtained by combining spectra collected from 5 min to 50 min into the run. *Panel D*, an observation mass spectrum of the DKO sample shown in Panel B was obtained by combining spectra collected from 5 min to 50 min into the run. The same ranges of the spectra as in *Panel C* were magnified for clarity. Note that the portions of the spectra in *Panel C* and *Panel D* from *m/z* 475 to *m/z* 775 and from *m/z* 775 to *m/z* 1200 were magnified × 2 and × 50, correspondingly, to compensate for their low intensity compared to the signal of cholesterol and cholesteryl esters with *m/z* 369.3538. All data were obtained in the APCI PIM ion mode. APCI, atmospheric pressure chemical ionization; PIM, positive ion mode.

Targeted supervised analysis of WT and double KO ML

The chemical nature of the analytes in WT and DKO samples was evaluated using their exact *m/z* values, elemental composition, fragmentation patterns, and UPLC retention times, and comparing those with authentic lipid standards (when available). The elemental composition of major lipid species (Table S1) was established using the EleComp software (Waters Corp) and verified using their fragmentation patterns in the MassLynx and the MS^E Data Viewer (all purchased through Waters Corp). The vast majority of the main MS signals in the WT samples originated from the typical very and extremely long chain (collectively dubbed hereafter as ELC) MLs (3, 14), while the majority of DKO signals were indicative of compounds of considerably shorter nature (Figs. 1 and 2).

As the total number of analytes in the TP samples (*i.e.*, potentially intact lipid species of interest or their fragments) exceeded a thousand entries, their comprehensive evaluation was considered impractical at this time and more focused approaches were chosen instead. All analytes that are reported in the paper for WT and DKO mice were compared using the

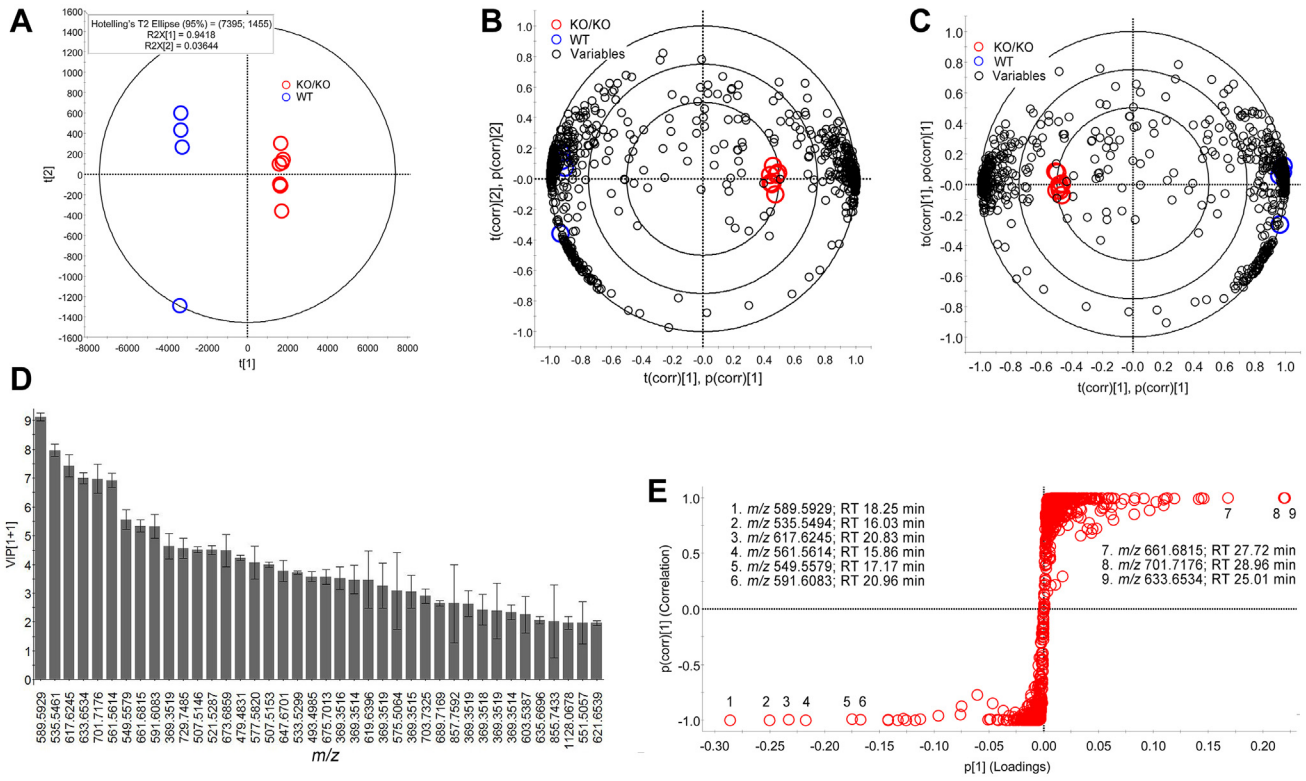

Figure 2. Multivariate statistical analyses of WT and double KO (DKO) Meibomian lipids. *Unbiased, untargeted principal component analysis (PCA)*: *Panels A,* a loadings plot of four WT (*blue dots*) and eight DKO (*red dots*) samples illustrated two clearly separated groups of DKO and WT samples. The intragroup differences were low, with one boarder-line outlier in the WT group. *Panel B,* a Loadings Bi-Plot allowed for identification of lipid analytes that were preferentially associated with either WT or DKO study samples. About 1012 variables (*i.e.*, analytes with unique combinations of *m/z* values and UPLC retention times) were detected by the Progenesis QI software. *Targeted Orthogonal Projections to Latent Structures Discriminant Analysis (OPLS-DA)*: *Panel C,* a Loadings Bi-Plot of the WT and DKO samples demonstrated excellent separation of the two groups of samples with associated analytes. *Panel D,* a variable importance plot (VIP) identified 40 most influential variables (*i.e.*, individual analytes) that determined the separation of WT and DKO study samples. Note extremely low standard errors for all 40 variables which indicate their high statistical significance. *Panel E,* data plotted as a S-Plot allowed for identification of the most influential analytes which were increased or decreased in the groups of samples. The analytes that grouped closest to the *bottom left corner* of the graph were the most prominent components of the WT samples, while the analytes in the *upper right corner* were specifically upregulated in the DKO samples. The distance from the center of the graph (X = 0; Y = 0) is proportional to the importance of the observations. All data were obtained in the APCI PIM ion mode. APCI, atmospheric pressure chemical ionization; PIM, positive ion mode; UPLC, ultra high performance liquid chromatography.

UPLC—MS peak areas calculated from their respective extracted ion chromatograms (EICs).

For the initial evaluation of the effects of the mutations, a several most abundant lipid species and lipid classes in meibum of both types of mice (selected from those shown in Figs. 1, 2, and Table S1) were chosen and compared. These lipids included free cholesterol (Chl) and CEs that share a common characteristic fragment with an *m/z* value of 369.3538 (dehydrated Chl; $C_{27}H_{45}$; a proton adduct), WEs with *m/z* values of 535.5457 (monounsaturated; $C_{36}H_{71}O_2$; a proton adduct), 617.6249 (diunsaturated; $C_{42}H_{81}O_2$; a proton adduct) and 619.6403 (monounsaturated; $C_{42}H_{83}O_2$; a proton adduct), and a TAG with an *m/z* value of 857.7576 (triunsaturated; $C_{55}H_{101}O_6$; a proton adduct). Their high-resolution mass spectra, obtained for WT and DKO samples, are shown in Figure 3, *A–F*. These results were typical of all tested samples and the lipid heat map highlighted the directions of changes caused by mutations.

When EICs of these lipids were plotted and the LC—MS peak areas determined (as shown for WEs $C_{36}H_{70}O_2$ and $C_{42}H_{82}O_2$ in Fig. 3, *G* and *H*) rather significant differences between the WT and DKO lipidomes became evident. The most striking observations for DKO mice included a ~2.5× increase in the combined pool of Chl and *total* CEs, more than a 10× increase in the amount of the shorter chain WE $C_{36}H_{70}O_2$, and a 20× increase in the diunsaturated WE $C_{42}H_{80}O_2$, with much more subtle changes (or no changes at all) in the production levels of the most common Meibomian-type monounsaturated WE $C_{42}H_{82}O_2$ and the TAG $C_{55}H_{100}O_6$ (Fig. 3*I*). The overall lipid production in the TPs of DKO mice, estimated using integrated TICs as described earlier (34), was 3 times that of WT mice ($p < 0.001$; Fig. 3*J*), which positively correlated with the increase in the physical size of DKO MGs (33).

The effects of the mutations on the unsaturation levels and elongation patterns of a series of major homologous Meibomian and sebaceous WEs were studied in more detail. The mean MS peak intensities were obtained by averaging WT and DKO raw files using the "Combine All Files" routine of the MassLynx software and observation spectra of both types of specimens were compared (Fig. 4, *A–D*). A preliminary analysis of the data confirmed a strong impact of the mutations on meibum but revealed a surprisingly weak effect on sebum. Note that unused Sebutape was used as control

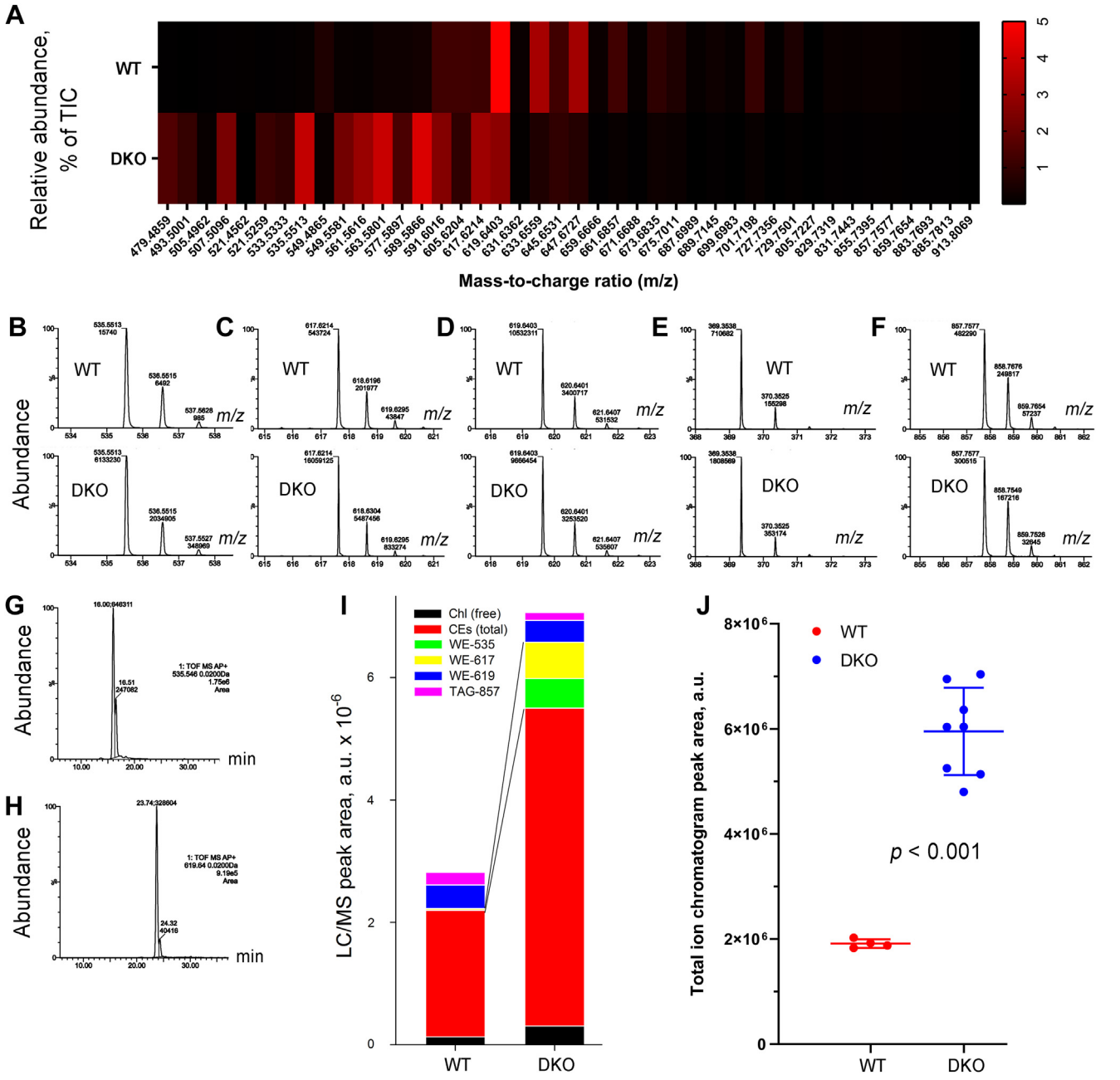

Figure 3. Targeted evaluative lipidomic analysis of a WT and a double KO (DKO) mouse tarsal plate samples. *Panel A,* a heat map of 42 major lipid analytes is shown. The data were normalized and are presented as percentages of the total ion count in the integrated total ion chromatogram. Note a considerable increase in the abundances of lower molecular weight (*i.e.*, shorter) analytes in the DKO sample. *Panels B–F,* high resolution mass spectra of matching pairs of five representative major lipids in WT and DKO samples were identical which confirmed their presence in both types of study samples. *Panels G* and *H,* extracted ion chromatograms of two representative analytes–a $C_{36}H_{70}O_2$ (a major wax ester in DKO samples) and a $C_{42}H_{83}O_2$ (a major wax ester in WT samples)–are shown. The LC—MS peaks were integrated and their LC retention times and peak areas are shown next to the peaks. Note that each compound eluted as two LC peaks with identical mass spectra, which indicates the existence of, at least, two isomeric forms of the compounds. *Panel I,* a side-by-side comparison of WT (4 samples, averaged data) and DKO (4 samples, averaged data) samples using absolute ion counts for each analyte. The numbers of tarsal plates per sample, sample dilutions, and sample injection volumes were identical for two types of samples. Major lipid species were compared–free cholesterol (Chl), total cholesteryl esters (CEs), three wax esters $C_{36}H_{70}O_2$ (WE-535), $C_{42}H_{80}O_2$ (WE-617), and $C_{42}H_{82}O_2$ (WE-619) and a triacylglycerol $C_{55}H_{100}O_6$ (TAG-857). *Panel J,* the total lipid production in four WT and eight DKO samples was compared using the total ion chromatogram (TIC) peak areas. The TIC peak areas of DKO samples, measured in identical conditions with WT samples, was 3 times of the latter. All spectra were recorded in the APCI PIM ion mode. APCI, atmospheric pressure chemical ionization; PIM, positive ion mode.

samples and contributed a MS peak with an *m/z* value of 663.4537 in PIM. Previously, this signal was identified as oxidized Irgafos 168 (35)–a derivative of a common plasticizer and a frequently found leachable in plasticware and organic solvents (36, 37).

The structures of major Meibomian WEs were verified using LC—MS as described earlier (14). Consistent with our earlier reports, main acyl moieties of WT Meibomian WEs were $C_{16:0}$, $C_{16:1}$, $C_{17:0}$, and $C_{18:1}$ fatty acids (FAs) followed by smaller amounts of other FAs. These FAs were observed in the

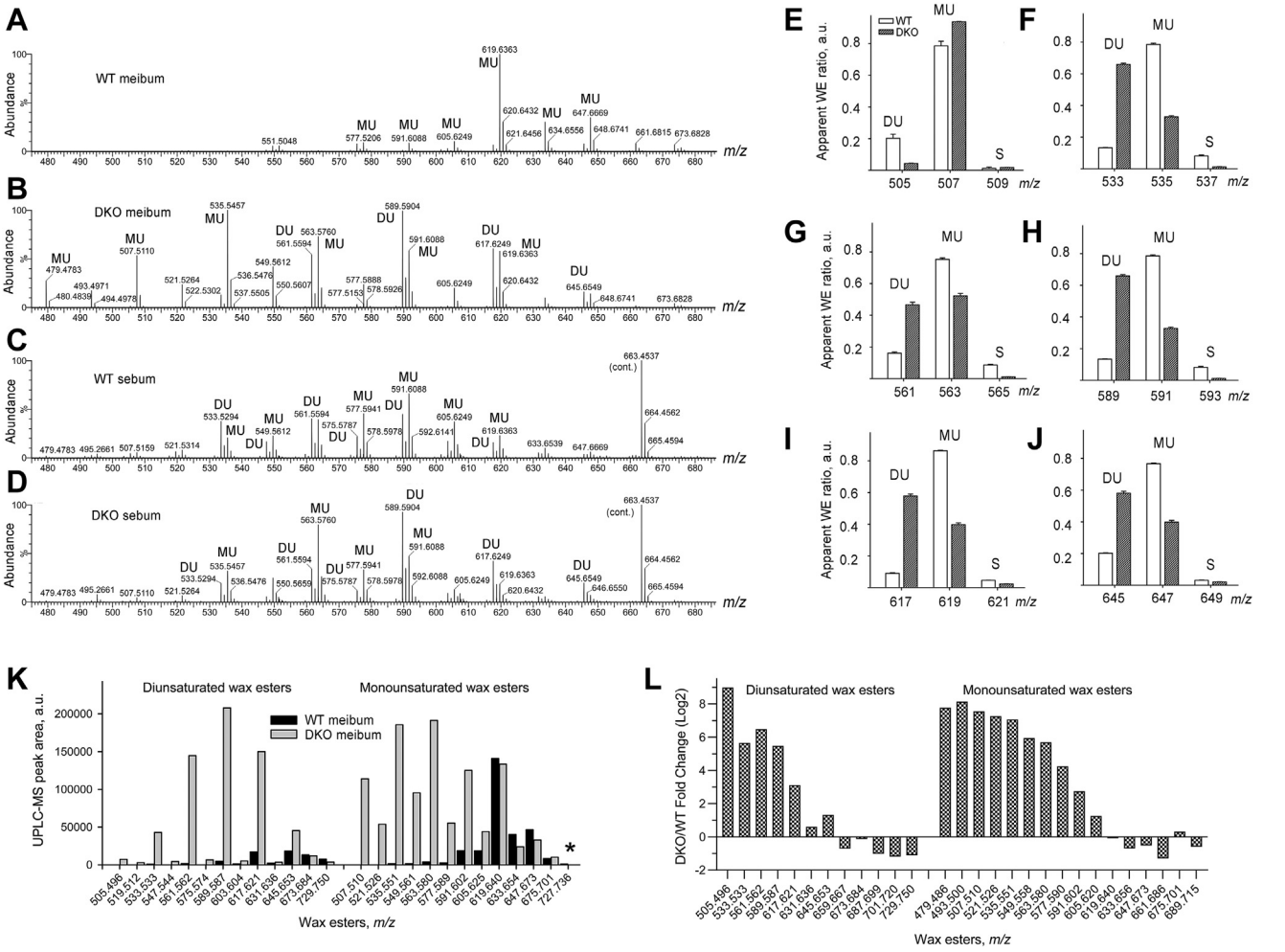

Figure 4. Characterization of the wax ester fractions of WT and double KO (DKO) meibum and sebum. *Panel A–D,* observation mass spectra of WT Meibomian lipids, DKO Meibomian lipids, WT sebaceous lipids, and DKO sebaceous lipids, correspondingly. Note the similarities between DKO Meibomian and WT/DKO sebaceous lipids. Major diunsaturated (DU) and monounsaturated (MU) WEs are labeled. (Cont.)–a ubiquitous contamination from plastic products and organic solvents (oxidized plasticizer Irgafos 168). *Panels E–J,* effects of the DKO mutation of *Sdr16c5* and *Sdr16c6* on the degree of unsaturation of mouse Meibomian WE. Relative ratios of major trios of DUWEs, MUWEs, and SWEs are shown. The total sum of three WEs in each graph equals 1. The exact *m/z* values and elemental compositions of WEs can be found in Table S1. All data were obtained in the APCI PIM. The differences between all matching pairs of signals for WT and DKO groups were statistically significant with $p < 0.05$ except for pairs of minor signals with *m/z* 509 (Panel *E*). *Panel K,* evaluation of the absolute amounts of major MUWEs and DUWEs in WT and DKO tarsal plate extracts. UPLC—MS peak areas of major tested WT and DKO Meibomian WEs. (*)–amount is too small for displaying purposes. *Panel L,* the DKO/WT WE fold changes undergo a sign change at monounsaturated WE $C_{42}H_{82}O_2$ and diunsaturated WEs $C_{44}H_{84}O_2$/$C_{45}H_{86}O_2$. APCI, atmospheric pressure chemical ionization; PIM, positive ion mode; UPLC, ultra high performance liquid chromatography.

current study for both WT and DKO TP specimens using the MS^E Data Viewer functionality of the MassLynx software (Fig. S3). Moreover, the MS^E approach allowed us to derive the carbon chain lengths of the fatty alcohol (FAL) moieties of WEs by calculating the difference between the $(M + H)^+$ adduct of a WE and its FA fragments. Note that the proton adducts of WEs fragmented to produce (M – fatty alcohol + $H)^+$ ions (*i.e.*, proton adducts of their FAs), which, subsequently, underwent spontaneous losses of two molecules of water, resulting in $(FA - H_2O + H)^+$ and $(FA - 2\times H_2O + H)^+$ adducts–useful fragments for confirmation of the FA structural assignments. The FAL carbon chain lengths varied from C_{16} to, at least, C_{32}, and largely determined the differences in the elongation patterns of WT and DKO MLs.

The mutations exerted only moderate effects on the chemical nature of the FA moieties of WEs: The apparent average ratios of the four major FA residues of WT and DKO WEs–$C_{16:1}$: $C_{16:0}$: $C_{17:0}$: $C_{18:1}$–were 0.20: 0.54: 0.17: 0.09, and 0.32: 0.42: 0.09: 0.16, correspondingly. Though the differences between the FA residues in the individual WT/DKO pairs were statistically significant ($p < 0.05$), they were not large enough to explain striking differences in the unsaturation levels and elongation profiles of WT and DKO WEs. Thus, it was determined that it was the FAL residues that were responsible for the changes in the elongation and unsaturation patterns of DKO WEs, with the main difference between WT and DKO meibum being the physical amounts of WEs of different lengths and their degrees of unsaturation.

Then, the EIC of six trios of saturated, monounsaturated-, and diunsaturated major homologous Meibomian WEs were plotted and integrated, to determine the UPLC—MS peak areas for each component, and their *relative* abundances were

normalized and plotted as shown in Figure 4, *E–J*. The data demonstrated a massive shift in the WE pool of the DKO lipidome toward diunsaturated compounds. The summation of all the peaks of diunsaturated WEs (DUWEs) and monounsaturated WEs (MUWEs) led to a conclusion that the original 24:76 (SD = 11%) ratio of DUWEs to MUWEs abundances in WT mice changed to 45:55 (SD = 15%) in their DKO littermates, while the *total* biosynthesis of 26 major DUWEs and MUWEs in DKO mice rose approximately 5 times. The pool of saturated WE (SWE) decreased in DKO mice, though their apparent abundance was low in mice with any genotype.

The trend of increasing the DUWEs/MUWEs ratio of in DKO samples was evident for all but the shortest WEs. Note that the signals of SWEs were low due to their poor ionizability under the conditions of UPLC—MS analysis, and, therefore, they are not discernible in Figures 1 and 4, *A–D*. However, when the data were plotted as EIC and normalized for each set of SWE, MUWE, and DUWE analytes (*e.g.*, the $C_{36}H_{72}O_2$, $C_{36}H_{70}O_2$, and $C_{36}H_{68}O_2$ pair of WEs) for each type of samples (*i.e.*, WT and DKO), so that the sum of abundances of each of the WE trios in each sample equaled 1, the fractions of SWEs in DKO samples were found to be significantly, and systematically, smaller than those in the WT samples, with the exception of the shortest trio of C_{34} WEs shown in Figure 4*E*.

A comparison of *absolute* amounts of major Meibomian WEs and their *fold changes* between WT and DKO genotypes was also conducted as shown in Figure 4, *K* and *L*. The UPLC—MS peak areas were determined for each analyte using integration of their EICs, which clearly illustrated the impact of mutations on the overall WE profiles (Fig. 4*K*). Note that the absolute amounts of shorter chain WE dominated the DKO samples, while longer chain WEs, starting with $C_{42}H_{82}O_2$, were ever so slightly lower in DKO specimens than in WT meibum. The tipping point for MUWEs was the major WE $C_{42}H_{82}O_2$, while in the group of DUWEs it was either $C_{44}H_{84}O_2$ or $C_{45}H_{86}O_2$ (Fig. 4*L*).

Next, changes in the pool of Meibomian CEs in response to mutations were studied (Fig. 5). Notably, not only the overall amounts of Chl and CEs in mouse TPs increased 2 to 3 times in response to inactivation of *Sdr16c5* and *Sdr16c6* genes, as it was already illustrated in Figure 3*I*, but the mutations caused noticeable changes in the CE profiles as well. Note the identical number of TPs per sample, sample volumes, LC—MS injection volumes, and data normalization of the graphs in Panels 5A and 5B, which allowed for an easy visual comparison of WT and DKO samples (Fig. 5*C*). As with WEs, the most obvious result of the mutation was an up-shift in the accumulation of various shorter chain CEs with FA carbon chain lengths in the $C_{12:0}$ to $C_{20:1}$ range, while most of ELC CEs with FAs longer than $C_{24:0}/C_{26:1}$ were in decline. A group of CEs with intermediate carbon chain lengths between $C_{19:0}$ and $C_{26:1}$ remained unchanged, with a notable exception of $C_{22:0}/C_{24:1}$ pair. The convoluted patterns of the changes in CE elongation profiles and the partial chromatographic overlap of the homologous saturated, monounsaturated, and diunsaturated CE trios with $C_{(n:0)}$, $C_{(n+2):1}$, and $C_{(n+4):2}$ FA residues made it impossible to evaluate them separately at this time, which is to be addressed in the future studies. However, when the apparent Chl/(Chl + all CEs) ratio was calculated for TP lipids of WT and DKO mice (Fig. 5*D*), no change in the efficacy of Chl esterification due to the mutations was observed ($p > 0.2$), but there were incremental declines in the Chl/total lipid and (all CEs)/total lipid ratios associated with the mutations ($p < 0.001$; Fig. 5*E*). A heatmap of major Meibomian CEs (Fig. 5*F*) provides numeric values for their ratios in the samples (with the total sum being 1). Surprisingly, the corresponding DKO/WT fold changes in individual CEs (Fig. 5*G*) were of a much smaller magnitude than the fold changes of WEs (Fig. 4*L*), which points toward a selective impact of the mutations on specifically WE biosynthesis (see Discussion).

Importantly, only trace amounts of squalene ($C_{30}H_{51}$; theoretical *m/z* 411.3991; experimental *m/z* 411.3978; a proton adduct) were found in all study specimens, with an apparent abundance of (0.004 ± 0.001)% of the total lipid pool, while no signals of retinol ($C_{20}H_{31}O$; theoretical *m/z* 287.2375; a proton adduct), its spontaneously in-source formed dehydration product dehydroretinol ($C_{20}H_{29}$; theoretical *m/z* 269.2269; a proton adduct), retinoic acid ($C_{20}H_{27}O_2$, *m/z* 299.2011, anion, analyzed in the negative ion mode), or retinaldehyde ($C_{20}H_{29}O$; theoretical *m/z* 285.2218; a proton adduct) were observed.

TAGs of the WT and DKO Meibomian lipidomes were also compared (Fig. 6, *A* and *B*), but no changes in the molecular profiles of TAGs caused by *Sdr16c5/Sdr16c6* inactivation were found as the mass spectra of both types of samples were virtually indistinguishable, with the same, highly repeatable elongation and unsaturation patterns. Notably, the overall *total amounts* of TAGs in each type of samples seemed to be almost identical, too: Note nearly equal total intensities of ions shown in Panels 6A and 6B for WT and DKO lipids, which were 3.67×10^4 and 3.52×10^4, respectively. When major TAGs in all individual WT and DKO samples were compared using their integrated EICs (Fig. 6*C*), there were no statistically significant differences found between the total amounts of TAGs per sample ($p > 0.8$; Fig. 6*D*), indicating no visible changes in the Meibomian TAG homeostasis in response to the mutations.

Comparison of mouse Meibomian and sebaceous lipids

Though it was possible to normalize Meibomian lipid production per TP and directly compare meibogenesis in WT and DKO mice in a semiquantitative manner, various experimental difficulties associated with measuring production of sebum in the mouse skin precluded us from estimating the effects of the mutations on sebogenesis. However, the *relative* amounts of sebaceous lipids in any given sample could be estimated using their MS abundances, and the intersample/interdonor comparisons were conducted as described below.

The inactivating mutations affected the pool of homologous sebaceous WEs (Fig. 7) to a much lesser extent than they did Meibomian WEs (Fig. 5). The Log(2) values of fold changes for

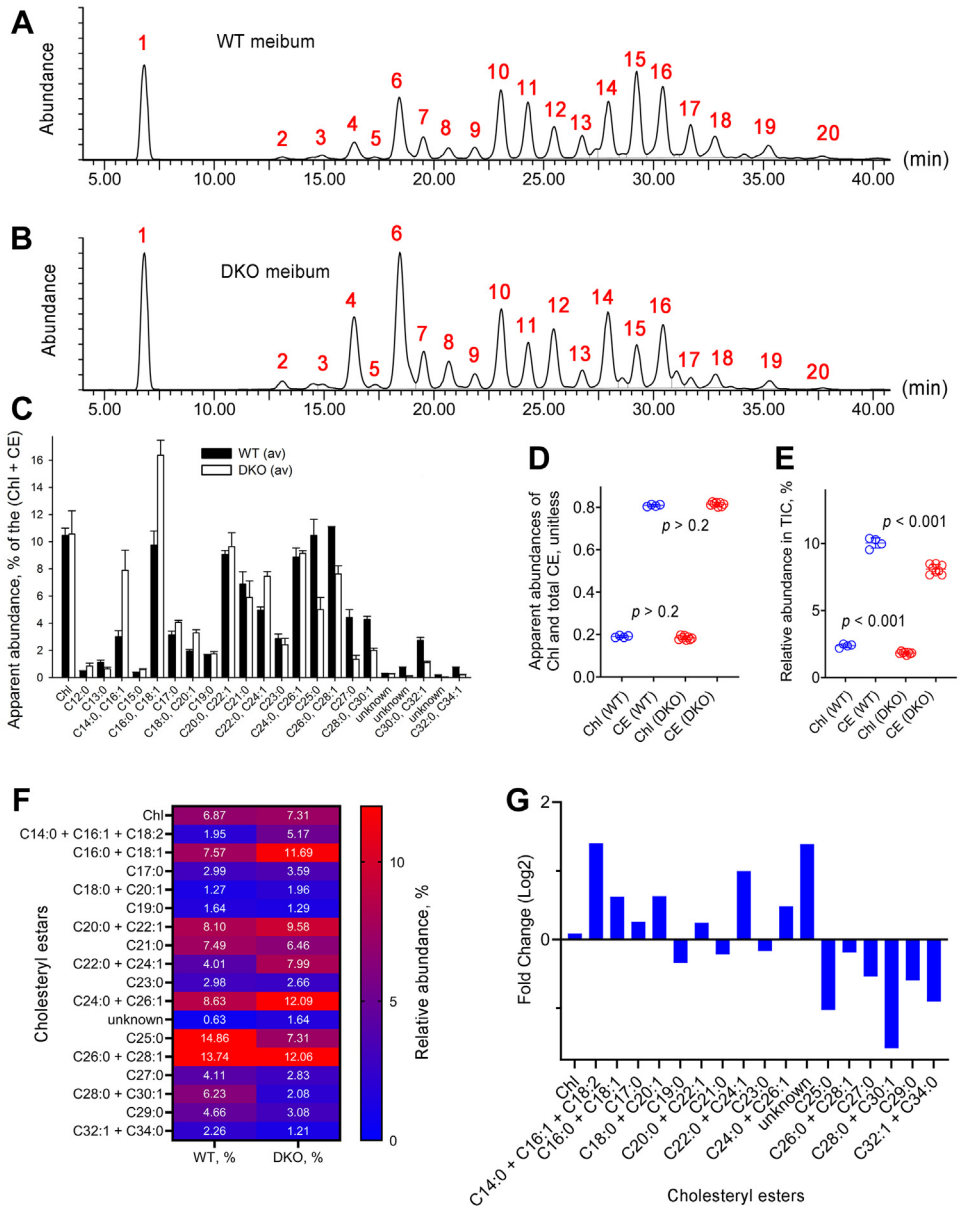

Figure 5. Effects of the double KO (DKO) mutations of *Sdr16c5* and *Sdr16c6* on the cholesteryl ester (CE) profile of Meibomian lipids. *Panel A,* representative extracted ion chromatogram of a common analytical ion of free cholesterol (Chl) and CEs with *m/z* value of 369.3538 obtained for a WT Meibomian lipid sample. Peak 1 – Chl; Peak 2 – $C_{12:0}$-CE; Peak 3 – $C_{13:0}$-CE; Peak 4 – $C_{14:0}$ + $C_{16:1}$ + $C_{18:2}$-CEs; Peak 5 – $C_{15:0}$-CEs; Peak 6 – $C_{16:0}$ + $C_{18:1}$-CEs; Peak 7 – $C_{17:0}$-CE; Peak 8 – $C_{18:0}$ + $C_{20:1}$-CEs; Peak 9 – $C_{19:0}$-CE; Peak 10 – $C_{20:0}$ + $C_{22:1}$-CEs; Peak 11 – $C_{21:0}$-CE; Peak 12 – $C_{22:0}$ + $C_{24:1}$-CEs; Peak 13 – $C_{23:0}$-CE; Peak 14 – $C_{24:0}$ + $C_{26:1}$- CEs; Peak 15 – $C_{25:0}$-CE; Peak 16 – $C_{26:0}$ + $C_{28:1}$-CEs; Peak 17 – $C_{27:0}$-CE; Peak 18 – $C_{28:0}$ + $C_{30:1}$-CEs; Peak 19 – $C_{30:0}$ + $C_{32:1}$-CEs; Peak 20 – $C_{32:0}$ + $C_{34:1}$-CEs. *Panel B,* representative extracted ion chromatogram of the common analytical ion *m/z* 369.3538 obtained for a DKO Meibomian lipid sample. Peak labels are the same as in Panel A. However, odd-numbered $C_{23:1}$-, $C_{25:1}$-, $C_{27:1}$, $C_{29:1}$, $C_{31:1}$, $C_{33:1}$, and $C_{35:1}$-CEs, though being minor CEs, were observed in DKO samples in considerably larger quantities than in WT samples. *Panel C,* apparent abundances of major CEs in WT and DKO samples. Total sum of all Chl and CE peaks equals 1. Data averaged for 4 WT and eight DKO samples are shown. *Panel D,* the apparent Chl/total CE ratio was the same for both types of the samples. ($p > 0.2$). *Panel E,* the relative abundances of Chl and total CEs, computed as the ratios of total Chl and total CE ions to total ion counts, were slightly higher in the WT samples ($p < 0.001$). *Panel F,* a heat map of major CEs. The total sum of signals equals 100%. *Panel G,* the DKO/WT CE fold changes did not exceed ±2 on a Log2 scale. All data were obtained in the APCI PIM. APCI, atmospheric pressure chemical ionization; PIM, positive ion mode.

all tested lipids were in the −2 to +2 range, with most of them being even smaller than that.

Sebaceous and Meibomian CEs of both genotypes were directly compared in a similar fashion (Figs. 5 and 8). Importantly, the profiles of Meibomian and sebaceous CEs bore no resemblance to each other with longer chain CEs dominating the former and shorter chain CEs forming the core of their sebaceous counterparts. The apparent ratios of sebaceous Chl and CEs were 42:58 for WT mice and 34:66 for their DKO littermates, *i.e.*, only minimal differences in the efficacy of Chl esterification were found ($p < 0.05$). The sebaceous CE profiles of two genotypes were also quite similar. However, the mutations caused a mild trend in the elongation profiles of sebaceous CEs that followed the Meibomian WE pattern: An

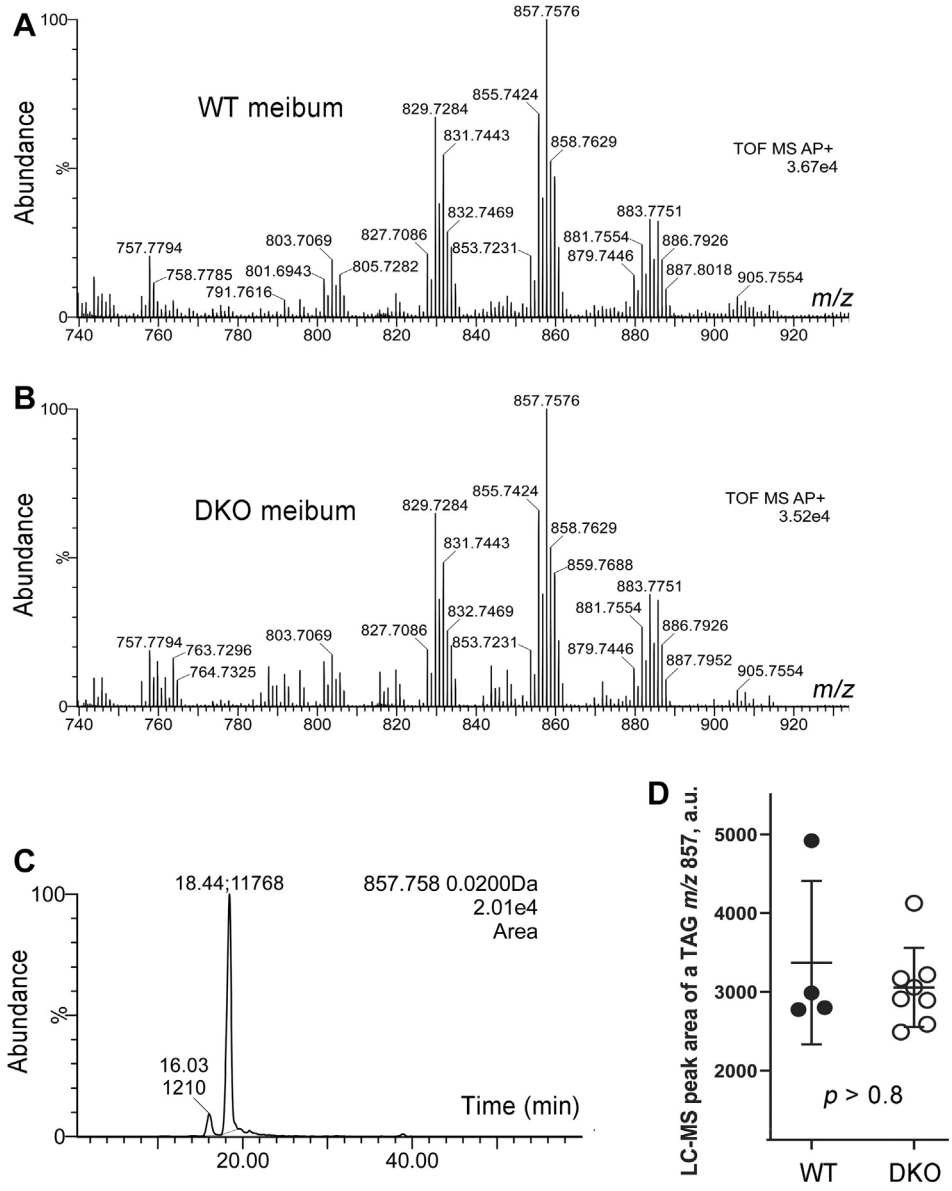

Figure 6. Triacylglycerols (TAGs) in WT and double KO (DKO) Meibomian lipid extracts. *Panel A,* the TAG fraction of a representative WT sample. *Panel B,* the TAG fraction of a representative DKO sample. *Panel C,* extracted ion chromatogram of a triunsaturated TAG $C_{55}H_{100}O_6$ with *m/z* 857.7576, its retention time (18.44 min) and peak area (11,768). A minor peak (16.03/1210) is an isotopic peak of a triunsaturated TAG $C_{55}H_{98}O_6$ with the main *m/z* 857.7576. Compounds were detected as $(M + H)^+$ adducts. *Panel D,* the TAG production in MGs of DKO mice was similar to that of WT mice ($p > 0.8$). Data for $C_{55}H_{100}O_6$ TAG is shown as an example. All data were obtained in the APCI PIM. APCI, atmospheric pressure chemical ionization; PIM, positive ion mode; MG, Meibomian gland.

increase in the apparent abundance of shorter chain CEs at the expense of the longer chain counterparts was observed, though the magnitude of this change was rather moderate.

Finally, the DKO TAG fractions in meibum and sebum did not endure any major compositional changes and were composed of regular TAGs of the C_{51}-C_{59} family.

Discussion

Earlier, simultaneous inactivation of *Sdr16c5* and *Sdr16c6* genes was shown to be associated with enlargement of sebaceous and Meibomian glands and a slit-eye phenotype in DKO mice, among other abnormalities (33). The lack of expression of the corresponding SDR16C5 and SDR16C6 proteins was demonstrated and explained by impaired retinol metabolism (*ibid.*). However, the effects of *Sdr16c5* and *Sdr16c6* inactivation on the biosynthesis of lipids in Meibomian and sebaceous glands (meibogenesis and sebogenesis, respectively) have not been explored before and became a subject of this publication.

The following considerations need to be re-emphasized before starting the discussion:

(1) The actual quantitation of several hundred lipid species found in meibum and sebum was not performed in this study as this would require the use of many dozens, if not hundreds, of lipid standards (preferably, isotopically labeled analogs), most of which are currently unavailable from any commercial sources;

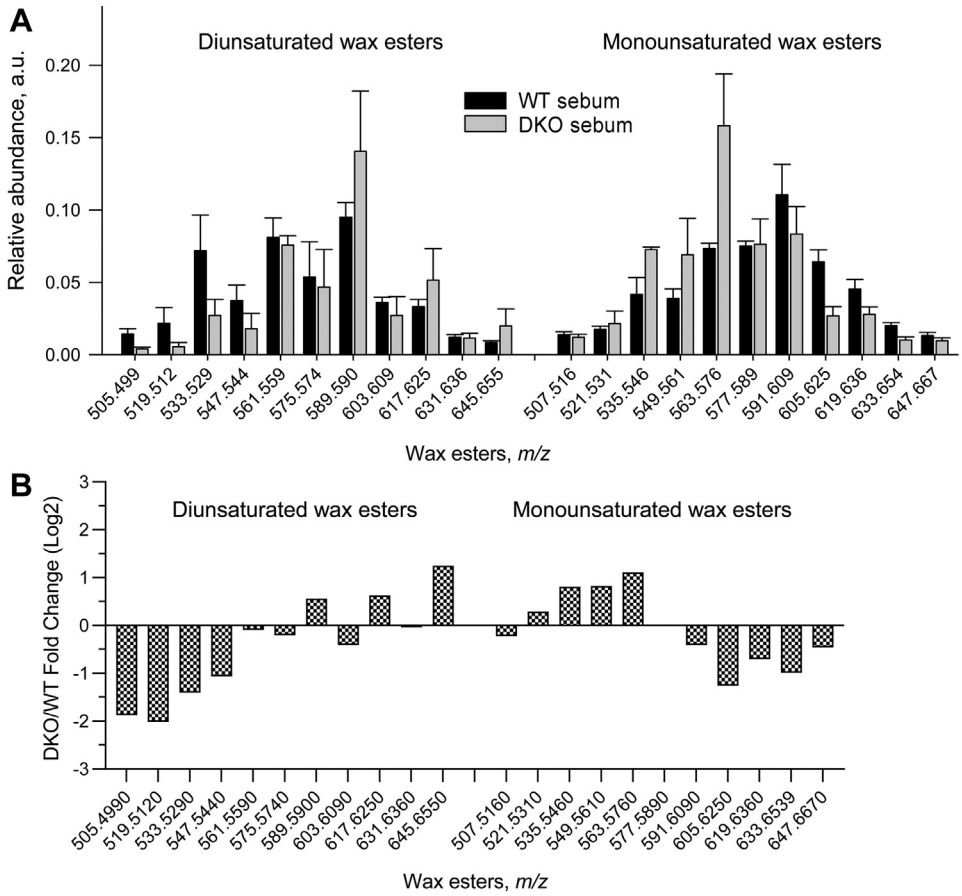

Figure 7. Targeted lipidomic analysis of a WT and a double KO (DKO) mouse sebum. *Panel A,* relative abundances of diunsaturated and monounsaturated wax esters in sebum demonstrated noticeable, but moderate, differences between the study groups. *Panel B,* the DKO/WT fold changes of major sebaceous WEs. All data were obtained in the APCI PIM. APCI, atmospheric pressure chemical ionization; PIM, positive ion mode.

(2) Even simplest metabolites, such as CEs and WEs, are present in sebum and meibum as mixtures of isomers that differ in FA and FAL carbon chain lengths, degree of unsaturation (*i.e.*, the number of double bonds), geometry of double bonds (*cis*- and *trans*-; conjugated and nonconjugated), geometry of FA and FAL ω-terminals (straight chain, *iso*-, or *anteiso*-), location of hydroxyl groups (ω-C, C2, or others), etc.;
(3) For the purpose of this study, we relied on the *apparent abundances* of analytes that were measured in LC—MS experiments as described in the Materials and Methods section of this paper; and
(4) For comparison purposes, the lipid production in WT and DKO MGs was normalized per TP, as measuring the weights of the tiny mouse TP specimens was found to be unreliable due to quick desiccation of the tissues during and after surgical excision from the mouse eyelids.

The most striking observations that were made when analyzing meibum and sebum of WT and DKO mice were a trifecta of (a) a considerable increase in the overall lipid production by MGs in mutant mice, (b) a massive shift in the lipid profile of DKO meibum that brought it closer to the lipid profile of sebum, and (c) only moderate changes in DKO sebum, which will all be discussed below.

Firstly, the overall production of meibum in WT and DKO mice was evaluated as described earlier for other types of mice (14, 16, 34) and found to be up to 3 times higher in DKO TPs than in WT TPs (Fig. 3*J*). This was consistent with the histological data on the enlargement of MGs in DKO mice that had been reported before (33) and was corroborated in this study as well. Thus, one could conclude that inactivation of the *Sdr16c5/Sdr15c6* pair of genes did stimulate biosynthesis of lipids in MGs of mutant mice.

Secondly, the increase in the amount of lipid produced by TPs was not caused by a straightforward activation of meibogenesis per se but was rather a result of a dramatic change in its products: When analyzing the overall mass spectra of the WT and DKO samples, one could see a shift in the DKO Meibomian lipidome toward the shorter chain, and less saturated, WEs (Figs. 1, 3 and 4). The tipping point of the change was a MUWE $C_{42}H_{82}O_2$ and DUWEs $C_{44}H_{84}O_2$/$C_{45}H_{86}O_2$, whose FA residues (after reduction to FAL by FAR1 or FAR2 and esterification by AWAT1/AWAT2) are likely products of sequential actions of ELOVL3, ELOVL1, and ELOVL4 (15–17). Indeed, we have previously demonstrated a similar shift in the WE profile of *Elovl3*-null mice, whose levels of ELC

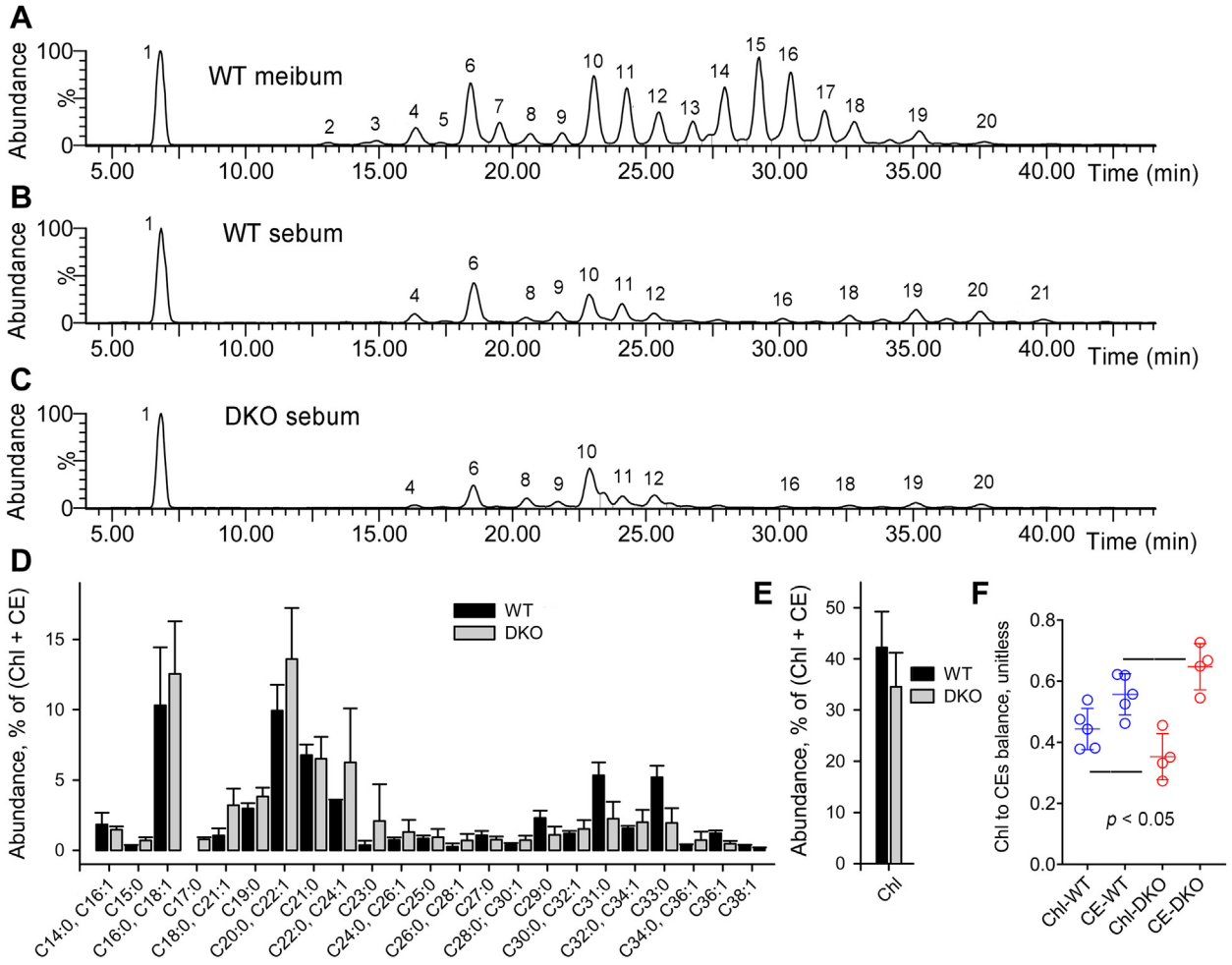

Figure 8. Targeted analysis of the cholesteryl ester (CE) profiles of WT and double KO (DKO) mouse sebaceous lipids. *Panel A,* a representative extracted ion chromatogram of a common analytical ion of free cholesterol (Chl) and cholesteryl esters (CEs) with *m/z* value of 369.3538 obtained for a WT sebaceous lipid sample in an APCI PIM experiment. Labeling of UPLC—MS peaks is the same as in Figure 5. *Panel B,* a representative extracted ion chromatogram of the common analytical ion *m/z* 369.3538 obtained for a WT sebaceous lipid sample. Labeling of UPLC—MS peaks is the same as in Figure 5. Peak 21 is a $C_{36:1}$-CE. Odd-numbered $C_{23:1}$-, $C_{25:1}$-, $C_{27:1}$, $C_{29:1}$, $C_{31:1}$, $C_{33:1}$, and $C_{35:1}$-CEs, though being minor CEs, were observed in sebum in considerably larger quantities than in meibum. *Panel C,* a representative extracted ion chromatogram of the common analytical ion *m/z* 369.3538 obtained for a DKO sebaceous lipid sample. *Panel D,* relative abundances of sebaceous major CEs in WT and DKO mice showed only minor effects of the mutations on the lipid balances. Note a change in the elongation patterns of CEs: If the FA lengths were shorter than C_{25}, the DKO CEs were expressed at higher levels than their WT counterparts, while the opposite was true for the C_{29}-FA and longer. *Panel E,* the abundance of Chl in the total (Chl + CEs) pool was incrementally higher in the WT mice ($p < 0.05$). *Panel F,* comparison of WT and DKO sebum samples demonstrated a moderate increase in the (total CE)/Chl ratio caused by the mutations. APCI, atmospheric pressure chemical ionization; PIM, positive ion mode; UPLC, ultra high performance liquid chromatography.

DUWEs and shorter-chain WEs increased due to the mutation, while SWEs were downregulated (16). Likewise, the levels of short-chain CEs were also increased, with the major change caused by saturated CEs. Importantly, the strength of the effect depended on the mouse zygosity, with *Elovl3*$^{+/-}$ samples showing all the trends at about 5 to 50% of the capacity of *Elovl3*$^{-/-}$ ones. Inactivation of *Elovl1* produced similar results but for a group of slightly longer lipids (17). Moreover, yet another enzyme of the FA elongation cycle–ELOVL4–may also be involved in this mechanism as it produces ELC FAs in the $>C_{26}$ range, which are essential components of many MLs. Thus, it seems plausible that the *Sdr16c5*/*Sdr16c6* genes (through the SDR16C5/SDR16C6 proteins they encode) may be responsible for controlling production of sebaceous-type WEs in MGs of mutant mice.

Thirdly, the pools of *sebaceous* WEs and CEs underwent much less significant changes in response to the double-gene KO (Figs. 7 and 8) than Meibomian WEs. The profiles of sebaceous WE species were altered in a rather complex manner, though the following trends emerged: Some of the shorter chain DUWEs were decreased in DKO samples, while longer chain DUWEs either increased or remained unchanged, with the WEs $C_{38}H_{72}O_2$ and $C_{39}H_{74}O_2$ being a tipping point for the change in the sign of the trend. Characteristically, the opposite trend was observed for MUWEs, with the same tipping point at WE $C_{39}H_{76}O_2$. In both cases, the 1- to 2-fold changes between identical pairs of sebaceous WT and DKO WEs were much lower than those of Meibomian WEs. For CEs, the trend was even more complex, with alternating patterns for ELC CEs (Fig. 5*G*). Due to their complexity, no attempts to characterize these changes in WEs and CEs in more detail were made at this time.

Thus, one can conclude that the mutations did not significantly affect the core reactions of meibogenesis but rather

lifted a barrier that controls the formation of sebaceous types of lipids, specifically WEs, and, to a degree, other types of lipids, in the TPs of mice.

A brief discussion on the possible reasons for these dramatic changes in the lipid profile of DKO meibum is warranted. A convenient starting point of the discussion is an observation that the CE profile of DKO meibum did not change much in response to the gene KOs, meaning that DKO MGs were still capable of elongating FAs to, at least, C_{32} or C_{34} (Fig. 5, *A*–*C*). The percentage of those ELC CEs in the total pool of CEs remained high (Fig. 5*F*), and the Chl/CE ratios (Fig. 5, *D* and *E*) were almost identical in both genotypes, which can be interpreted as the lack of a major impact of the mutations on selectivity of the Chl esterification reactions, except for 1- to 2-fold increase in the relative abundance of regular C_{14}—C_{18} CEs. However, the *total* amount of all CEs formed in DKO MGs was 2 to 3 times higher than that in WT MGs (2.5, on average). These observations implied that: (1) large amounts of long chain and ELC FAs were still available for meibogenesis; (2) the amount of ELC FAs available for esterification of Chl in DKO MGs was, at least, no smaller than in WT MGs; and (3) inactivation of *Sdr16c5/Sdr16c6* had a stronger impact on the overall *capacity* of the CE subpathway of meibogenesis, rather than its product specificity.

Another important fact is the production of Meibomian ELC MUWEs, which also remained high (Fig. 4*A*). Note that the graph illustrates the UPLC-MS peak areas for the corresponding WE species, which allows to directly compare the *total* production of these metabolites in DKO and WT TP specimens due to the identical analytical conditions. Therefore, a conclusion can be made that TPs of DKO mice did not lose the ability to produce almost normal amounts of ELC WEs (per TP), but, on top of that, gained the ability to produce shorter chain and DUWE in copious amounts.

The profiles of Meibomian and sebaceous CEs of WT and DKO mice were also compared and some common trends were observed. In particular, the changes in the CE elongation profiles of DKO meibum and sebum paralleled each other (Figs. 5 and 8). Two general trends for both meibum and sebum DKO specimens were an increase in some shorter chain CEs and a decline in ELC CEs with a tipping point laying in the C_{22}—C_{24} FA chains lengths range. This observation ruled out any major effect of *Sdr16c5/Sdr16c6* inactivation on the Chl and CE profiles in sebum, while demonstrating its much stronger effect on meibogenesis.

Once the lipid production was normalized per TP, the overall amount of lipids detected in DKO mice was found to be ~3 times higher than that in WT mice (Fig. 3*J*). The increase originated, in part, from shorter-chain, and more unsaturated, sebaceous-type C_{20} to C_{40} WEs, which are found in WT meibum only in small quantities (Figs. 3 and 4). At the same time, inactivation of *Sdr16c5* and *Sdr16c6* produced a massive rise in diunsaturated Meibomian WEs of DKO meibum, which are a rather small group of lipids in WT mouse meibum. These observations clearly implicate *Sdr16c5* and *Sdr16c6* in regulating the WE subpathway of meibogenesis, either by affecting its FA desaturation, elongation cycles, and/or reduction cycles or by controlling FA, FAL, and Chl condensation into WEs and CEs. Importantly, inactivation of *Sdr16c5* and *Sdr16c6* had no major impact on the formation of Meibomian-type WEs as the elongation profiles of WEs longer than C_{42}, and their production levels per TP, barely changed (Fig. 4). Therefore, one can conclude that mutations had a profound, but a convoluted, effect on meibogenesis by affecting lipid profiles of MLs.

Interestingly, inactivation of *Sdr16c5/Sdr16c6* brought the mass spectra of DKO MG lipids closer to those that were reported for human sebum and abnormal human meibum collected from a patient with "High Triglycerides-Low Waxes" syndrome (HTLW) (28) and WT and DKO mouse sebum. Indeed, the HTLW meibum was enriched with shorter chain WEs in the C_{30} to C_{40} range, and CEs with C_{14}—C_{18} long-chain FAs (LC FA) residues, though its total DUWE to MUWE ratio declined.

The LC FAs are found in all classes of MLs. Among those, WEs and CEs are the main lipids that comprise the majority of the Meibomian lipid pool. In WEs, the main FAs moieties are $C_{16:0}$, $C_{16:1}$, $C_{17:0}$, $C_{18:0}$, and $C_{18:1}$ FAs, esterified to, mainly, ELC FALs with the carbon chain lengths ranging from C_{20} to C_{34}, while in CEs the FA residues also change from C_{12} to C_{34} (Fig. 5). The relative abundance of Meibomian LC FAs (those from C_{12} to C_{21} or so) in the WE and CE pools went up in DKO mice, as Figures 3 and 5 illustrate, but their actual molar concentrations in the specimens have not been determined at this time because of the lack of chemical standards for the vast majority of MLs.

Importantly, the STRING database (https://www.string-db.org; accessed March 22nd, 2023) lists mouse *Sdr16c5* as a part of a cluster with *Awat2* and several forms of alcohol dehydrogenases, such as *Aldh1a1, Aldh1a2, Aldh1a3, and Aldh1a7* and other functionally similar genes, because of their possible association and co-expression in the mouse epidermis. Similar relationships are expected for their human counterparts as well. Two mouse wax synthases were originally described by Cheng and Russell in 2004 (22). One year later, Turkish *et al.* characterized human AWAT1 and AWAT2 *in vitro* using their overexpression in yeasts and determined that the enzymes have distinctively different substrate specificities (38). However, the enzymes were studied with relatively short FALs in the C_{10} to C_{20} range, while the typical range of Meibomian FALs extends to C_{34} or more. Therefore, their preferences toward ELC FALs and FAs remained unknown. The substrate/product specificities of AWAT1 and AWAT2 were recently evaluated by McMahon *et al.* (23), Widjaja-Adhi *et al* (24), and Sawai *et al.* (39) who reported their complex and differential effects on the specificity of the biosynthesis of WEs and other types of Meibomian ester lipids. Importantly, genes of the *Awat, Aldh,* and *Sdr* families are highly expressed in mouse MGs (data reanalyzed from the National Center for Biotechnology Information Gene Expression Omnibus dataset GSE78499 found at https://www.ncbi.nlm.nih.gov/geo/query/acc.cgi?acc=GSE78499; also reported in independent publications (14, 24, 26, 39, 40)), which alludes to their important roles in the MG lipid homeostasis. As ALDHs are essential for converting fatty aldehydes into FAs (oxidizing, for example,

retinaldehyde into retinoic acid) (41–43)), we hypothesize that these enzyme(s) may have the same function in MGs, working in concert with SDR16C5/SDR16C6, FAR1/FAR2, and AWAT1/AWAT2 in a FAL ⇄ fatty aldehydes ⇄ FA ⇄ FAL conversion cycle (Fig. 9).

Indeed, our recent mRNA microarray and single-cell RNA seq experiments demonstrated that both *Sdr16c5* and *Awat2* genes are co-expressed at high levels in several cell clusters in MGs of mice (26), while our current experiments revealed that their concerted actions are critical factors in WE metabolism in MGs. Thus, the functional association of these genes may be extended beyond skin and sebocytes to MGs and meibocytes of mice. Considering that SDR16C5/SDR16C6 have been implicated in regulation of the retinoid metabolism (33, 44), it was logical to assume that a retinoid signaling pathway, similar to those proposed earlier (45–47) might be involved in meibogenesis. However, considering (1) the current lack of evidence of the presence of retinoids among MG lipids and (2) a very high level of expression of *Sdr16c5/Sdr16c6* in MGs of mice, which is on par with other major genes of meibogenesis that are responsible for biosynthesis of main components of meibum (such as *Elovl1, Elovl3, Elovl4, Scd1, Scd3, Far2, Dhcr24, Soat1, Awat1, Awat2,* and *Dgat2*, among others), it is highly plausible that SDR16C5 and/or SDR16C6 are involved in the direct production of MLs as catalysts of one of the critical steps of meibogenesis. This function of SDR16C5/

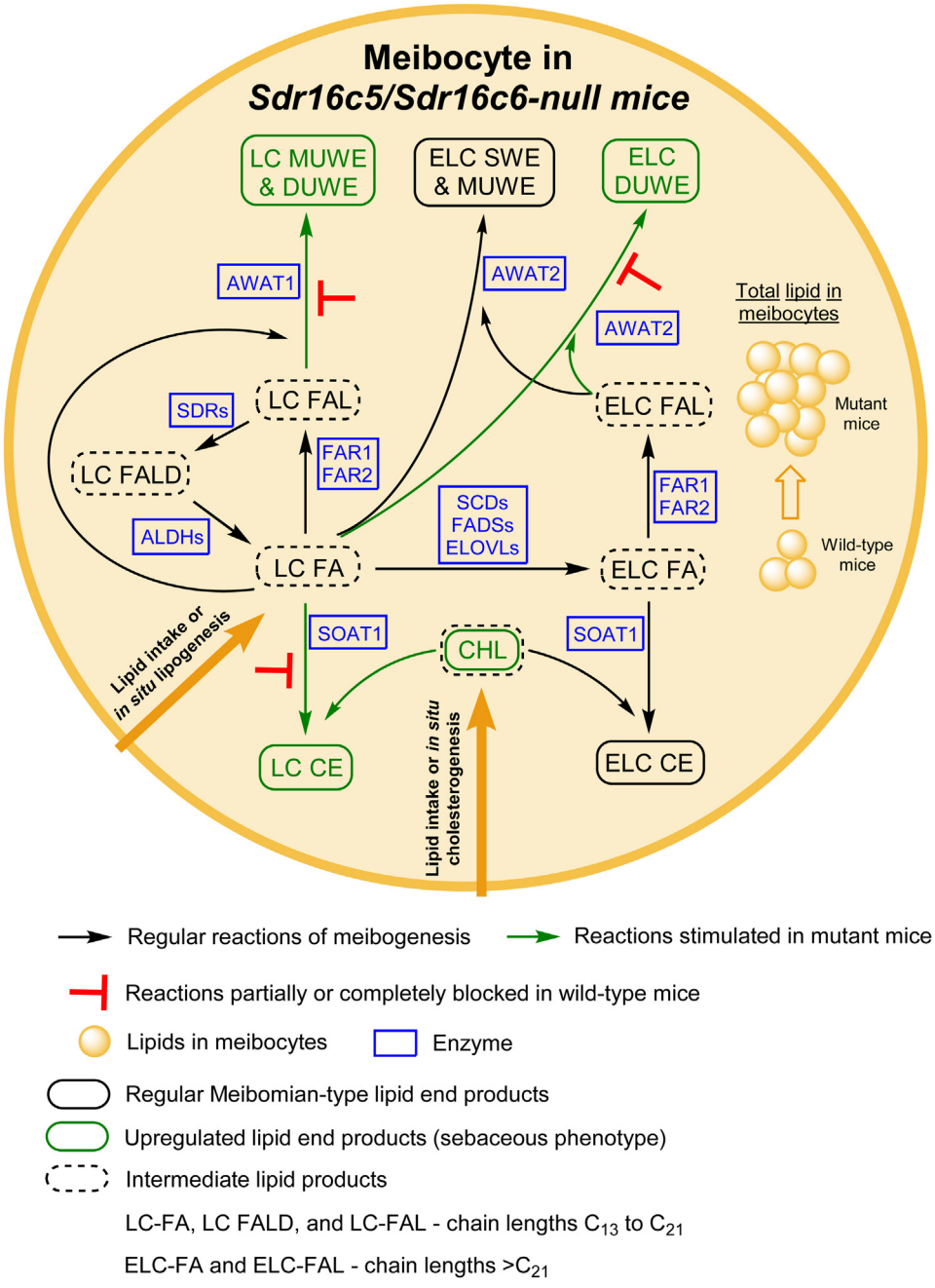

Figure 9. A proposed mechanism of *Sdr16c5/Sdr16c6* regulation of meibogenesis in mice.

SDR16C6 has not been proposed and explored before. Importantly, the mice deficient in solely SDR16C6 did not produce any abnormal ocular phenotype (33), meaning that either this enzyme is not involved in meibogenesis or the activity of SDR16C5 is sufficient for maintaining lipid homeostasis in the eye and adnexa. These possibilities are to be tested in future experiments.

Summarizing these observations, we conclude that ablation of the *Sdr16c5/Sdr16c6* pair of mouse genes seems to trigger an additional, previously dormant but potent, sebaceous-type biosynthetic subpathway that was silent in WT MGs, but became active in MGs of DKO mice, with a rather moderate impact on the normal subpathways of meibogenesis. This resulted in a considerable shift in the lipid profiles of MLs and the increase in the total amount of meibum produced by MGs. The overall effects of the *Sdr16c5/Sdr16c6* inactivation on WE and CE subpathways of meibogenesis are recapitulated and summarized in Figure 9. We propose that these genes may act as gatekeepers controlling, among other possible functions, specificity of WE and, to a lesser extent, CE biosynthesis. We are confident that future studies will unravel the intricate mechanisms of their action in MGs and answer a question about their potential therapeutic role as targets for correcting abnormal meibum composition, or meibum deficiency, in humans with various Meibomian gland abnormalities (28, 48) or systemic lipid disorders.

Experimental procedures

Reagents

Authentic lipid standards were purchased from MilliporeSigma, Avanti Polar Lipids, Inc, and NuChek Prep., Inc. Acetic and formic acids (both >99.9% pure) and ammonium formate (>99.995%) were from MilliporeSigma. Organic solvents, such as *iso*-propanol (IPA), acetonitrile, chloroform, and methanol were of chromatography- or MS-grade from MilliporeSigma and Thermo Fisher Scientific. Ultra high purity compressed gasses (helium and nitrogen) were from Airgas.

Animal procedures and sample preparation

Generation of the *Sdr16c5*$^{-/-}$*and Sdr16c6*$^{-/-}$ DKO mice has been described in (33). Mice were housed in the University of Alabama AALAC-approved animal facility with free access to water and food (standard rodent chow diet obtained from Harlan, catalog number 7017) with a light cycle of 12 h light and 12 h dark. The DKO strain used in this study (DKO1 in the original publication (33)) harbors a single deletion, inactivating both genes. The original strain underwent eight rounds of backcrossing to the WT C57BL6/6J mice. Mice heterozygous for the DKO allele were crossed to obtain WT and DKO littermates. These littermates were used as breeders to generate WT and DKO experimental animals. Age-matched 6-month-old animals of both sexes were used for lipidomic analyses. The animals were euthanized with carbon dioxide inhalation followed by cervical dislocation, chilled, and shipped the same day on ice to the University of Texas Southwestern Medical Center using an overnight delivery service.

TPs were excised under a Zeiss Stemi 508 dissecting microscope featuring a Zeiss CL 6000 LED light source (Zeiss), surgically separated from other ocular tissues, and the lipids were extracted from all four TPs/mouse with a chloroform/methanol = 2/1 (v/v) solvent mixture (CM21) as described before (26). The TP samples were not weighed because of their small size and rapid desiccation at typical room temperature and humidity. The lipid extracts from individual mice were redissolved in 0.5 ml of IPA in a 2-mL glass HPLC-autoinjector vials crimped with Teflon-lined caps and stored at −20 °C until the analyses.

Mouse sebum samples were collected from preshaved skin on the back of the animals using Sebutape [from Clinical and Derm LLC (formerly CuDerm)], simultaneously with collecting their TPs. The lipids were extracted from Sebutape using a 3 × 2.5 ml extraction with *n*-hexane/IPA = 1:1 (v/v) solvent mixture, the three extracts were pooled, brought to dryness under a stream of nitrogen, the oily residue was redissolved in 1 ml of IPA, and the sample was stored as described above for TP specimens.

Lipidomic analyses of samples using chromatography and MS

Lipidomic analyses were conducted using a high-resolution quadrupole Time-of-Flight Synapt G2-Si mass spectrometer equipped with either an IonSabre-II APCI or an electrospray ionization Low-Flow ion sources and a ZSpray/LockSpray unit (all from Waters Corp). A NitroFlow Lab nitrogen generator was from Parker Balston. The Leucine-Enkephalin was used as a reference LockSpray reagent for continuous in-line corrections of the mass spectra. Experiments were conducted, depending on the application, in either sensitivity mode (R ≥ 10,000 FWHP) or high resolution (R ≈ 40,000 FWHP) mode, with a mass error of, typically, between 1 and 10 mDa in the *m/z* range of 100 to 2000 amu. The system was operated using the MassLynx software v.4.1 (from Waters).

A UPLC Acquity M-Class system composed of a μ-Sample Manager-FL, a μ-Binary Solvent Manager, an Auxiliary Solvent Manager, and a Trap Valve Manager (all from Waters. Co.) was used to run UPLC experiments. Two types of UPLC chromatographic columns were used–a 2.1 mm × 100 mm C8 BEH Acquity column with 1.7 μm particles and a 1.0 mm × 100 mm C18 BEH Acquity column with the same particle size (both from Waters Co.). Both columns were thermostated at 35 °C during the analyses. The C8 column was used in combination with isocratic elution of the lipid analytes with 95% IPA/5% of 10 mM aqueous ammonium formate at a 16 μl/min flow rate, while the C18 column was used for gradient elution of the analytes with an acetonitrile/IPA/5% of 10 mM aqueous ammonium formate solvent mixture as described earlier (34). Between 0.5 and 4 μl of sample, solutions were injected. Reproducibility of the analyses and the linearity of the instrument response was verified as described before for similar samples (34). The SDs for multiple injections of the same samples did not exceed 5% and the instrument's responses were linear or quazi-linear in the used concentration ranges.

Data analysis and statistical considerations

Lipidomic analyses were conducted in the MassLynx and the Progenesis QI software packages (from Waters Corp). The raw files were imported in MassLynx and evaluated as TIC and combined observation mass spectra (as illustrated in Fig. 1).

Then, an unbiased approach was used to compare the study samples and determine analytes that differed most significantly between the WT and DKO study samples. The raw LC—MS files were imported into Progenesis QI, processed using its built-in algorithms, and exported to EZinfo (from Waters Corp/Umetrics) for further analyzing using its PCA and OPLS-DA templates.

The nature of all lipid analytes described in this paper was established in previous projects and reported in a series of publications (14, 49). Briefly, the structures of the lipid analytes were determined using their high-resolution *m/z* values obtained with mass errors of routinely better than 5 mDa for all major lipids, their MS/MS and MS^E fragmentation patterns, and UPLC retention times, all compared with authentic lipid standards (when available).

Then, compounds of interest were analyzed using a more targeted approach. Their EIC obtained with, depending on an application, a mass window of 0.01 to 0.05 Da, were integrated using the MassLynx's "Integrate" subroutine, and the calculated UPLC—MS peak areas were used to compare the apparent abundances of the analytes in the samples. Note that the apparent abundances of the analytical ions are proportional to their concentrations in the study samples, but depend on the efficacy of ionization of lipids in the ion source of the mass spectrometer, and vary from class to class or even within any given class for series of homologous lipids. Thus, the most practical and prudent way of analyzing the data was to use the absolute or relative abundances of the lipids and compare them side-by-side for WT and DKO samples analyzed in identical experimental and postexperimental conditions.

When applicable, all the experimental conditions, including the number of the excised and extracted TPs, the final volumes of solutions of extracted lipid samples, LC—MS injection volumes, and mass spectrometric and chromatographic parameters were kept constant, which facilitated easier comparisons of WT and DKO study samples.

To accommodate for different scenarios, two types of comparisons were used–an intrasample balance of different lipids, expressed as their normalized abundances (on a 0% to 100%, or 0–1 scales) or their absolute ion counts (changing from 0 to ∞). Note that the normalized abundances of ions is a default setting of the MassLynx software and a de facto industry standard for presenting complex MS data.

Statistical analyses of the data were performed in SigmaStat v.11.0 and SigmaPlot v.3.5 software packages (from Systat Software, Inc) and GraphPad Prism 8.0.2 (from GraphPad Software, Inc). The matching lipid pairs from WT and DKO samples were compared using the Student's *t* test (for the samples that passed the normality test) or the Mann-Whitney Rank Sum test (for those that failed the normality test). The differences with *p*-value of ≤0.05 were considered statistically significant.

Study approval

All animal-related procedures were approved by the Institutional Animal Care and Use Committees of the University of Texas Southwestern Medical Center and University of Alabama. The animals were treated in accordance with the Association for Research in Vision and Ophthalmology Statement for the Use of Animals in Ophthalmic and Vision Research.

Data availability

All pertinent data are included in the manuscript.

Supporting information—Supplemental Table S1; Supplemental Figures S1, S2, and S3. This article contains supporting information.

Acknowledgments—None.

Author contributions—I. A. B. methodology; I. A. B. supervision; I. A. B., S. Y., and A. W. formal analysis; I. A. B. writing-original draft; I. A. B., N. Y. K., K. R. G., and O. V. B. resources; I. A. B., A. W., K. R. G., O. V. B., N. Y. K., and S. Y. writing-reviewing and editing; I. A. B., A. W., and S. Y. investigation.

Funding and additional information—The project was supported in part by US National Institutes of Health Grants R01 EY024324 and R01 EY027349 (to I. A. B.) and R01 AA012153 (to N. Y. K.).

Conflict of interest—The authors declare that they have no conflicts of interest with the contents of this article.

Abbreviations—The abbreviations used are: APCI, atmospheric pressure chemical ionization; CE, cholesteryl ester(s); DKO, double KO; DUWE, diunsaturated WE(s); EIC, extracted ion chromatogram; ELC, extremely long chain; FA, fatty acid(s); FAL, fatty alcohol(s); FAR, fatty acid reductase; IPA, iso-propanol; LC FA, long-chain FA(s); MG, Meibomian gland(s); ML, meibomian lipid(s); MUWE, monounsaturated WE(s); OPLS-DA, Orthogonal Projections to Latent Structures Discriminant Analysis; PCA, Principal Component Analysis; PIM, positive ion mode; SWE, saturated WE(s); TAG, triacyl glycerol(s); TIC, total ion chromatogram; TP, tarsal plate(s); UPLC, ultra high performance liquid chromatography; WE, wax ester(s).

References

1. Meibom, H. (1666) De Vasis Palpebrarum Novis Epistolae, Henningi Mulleri, Helmstadt, Germany
2. Nicolaides, N., Kaitaranta, J. K., Rawdah, T. N., Macy, J. I., Boswell, F. M., 3rd, and Smith, R. E. (1981) Meibomian gland studies: comparison of steer and human lipids. *Invest. Ophthalmol. Vis. Sci.* **20**, 522–536
3. Butovich, I. A. (2017) Meibomian glands, meibum, and meibogenesis. *Exp. Eye Res.* **163**, 2–16
4. Bron, A. J. (1988) Eyelid secretions and the prevention and production of disease. *Eye (Lond)* **2**, 164–171
5. Linton, R. G., Curnow, D. H., and Riley, W. J. (1961) The meibomian glands: an investigation into the secretion and some aspects of the physiology. *Br. J. Ophthalmol.* **45**, 718–723
6. Andrews, J. S. (1973) The Meibomian secretion. *Int. Ophthalmol. Clin.* **13**, 23–28
7. Iwata, S., Lemp, M. A., Holly, F. J., and Dohlman, C. H. (1969) Evaporation rate of water from the precorneal tear film and cornea in the rabbit. *Invest. Ophthalmol.* **8**, 613–619

8. Holly, F. J. (1973) Formation and rupture of the tear film. *Exp. Eye Res.* **15**, 515–525
9. Holly, F. J. (1973) Formation and stability of the tear film. *Int. Ophthalmol. Clin.* **13**, 73–96
10. McCulley, J. P., and Sciallis, G. F. (1977) Meibomian keratoconjunctivitis. *Am. J. Ophthalmol.* **84**, 788–793
11. Holly, F. J. (1985) Physical chemistry of the normal and disordered tear film. *Trans. Ophthalmol. Soc. U K* **104**, 374–380
12. Kilp, H., Schmid, E., Poss, W., and Kirchner, L. (1985) Changes of the tear film in dry eyes. *Trans. Ophthalmol. Soc. U K* **104**, 450–451
13. Franck, C. (1991) Fatty layer of the precorneal film in the 'office eye syndrome. *Acta Ophthalmol.* **69**, 737–743
14. Butovich, I. A., McMahon, A., Wojtowicz, J. C., Lin, F., Mancini, R., and Itani, K. (2016) Dissecting lipid metabolism in meibomian glands of humans and mice: an integrative study reveals a network of metabolic reactions not duplicated in other tissues. *Biochim. Biophys. Acta* **1861**, 538–553
15. McMahon, A., Lu, H., and Butovich, I. A. (2014) A role for ELOVL4 in the mouse meibomian gland and sebocyte cell biology. *Invest. Ophthalmol. Vis. Sci.* **55**, 2832–2840
16. Butovich, I. A., Wilkerson, A., Bhat, N., McMahon, A., and Yuksel, S. (2019) On the pivotal role of Elovl3/ELOVL3 in meibogenesis and ocular physiology of mice. *FASEB J.* **33**, 10034–10048
17. Sassa, T., Tadaki, M., Kiyonari, H., and Kihara, A. (2018) Very long-chain tear film lipids produced by fatty acid elongase ELOVL1 prevent dry eye disease in mice. *FASEB J.* **32**, 2966–2978
18. Anderson, G. J., and Kolattukudy, P. E. (1985) Fatty acid chain elongation by microsomal enzymes from the bovine meibomian gland. *Arch. Biochem. Biophys.* **237**, 177–185
19. Miyazaki, M., Man, W. C., and Ntambi, J. M. (2001) Targeted disruption of stearoyl-CoA desaturase1 gene in mice causes atrophy of sebaceous and meibomian glands and depletion of wax esters in the eyelid. *J. Nutr.* **131**, 2260–2268
20. Kolattukudy, P. E., and Rogers, L. (1986) Acyl-CoA reductase and acyl-CoA: fatty alcohol acyl transferase in the microsomal preparation from the bovine meibomian gland. *J. Lipid Res.* **27**, 404–411
21. Cheng, J. B., and Russell, D. W. (2004) Mammalian wax biosynthesis. I. Identification of two fatty acyl-Coenzyme A reductases with different substrate specificities and tissue distributions. *J. Biol. Chem.* **279**, 37789–37797
22. Cheng, J. B., and Russell, D. W. (2004) Mammalian wax biosynthesis. II. Expression cloning of wax synthase cDNAs encoding a member of the acyltransferase enzyme family. *J. Biol. Chem.* **279**, 37798–37807
23. McMahon, A., Yuksel, S., Bhat, N., Pham, H., Wilkerson, A., and Butovich, I. A. (2020) Inactivation of Awat2 in mice causes loss of wax ester lipids from meibum. *Invest. Ophthalmol. Vis. Sci.* **61**, 2632
24. Widjaja-Adhi, M. A. K., Silvaroli, J. A., Chelstowska, S., Trischman, T., Bederman, I., Sayegh, R., *et al.* (2020) Deficiency in Acyl-CoA:Wax Alcohol Acyltransferase 2 causes evaporative dry eye disease by abolishing biosynthesis of wax esters. *FASEB J.* **34**, 13792–13808
25. Butovich, I. A., Wilkerson, A., and Yuksel, S. (2021) Depletion of cholesteryl esters causes meibomian gland dysfunction-like symptoms in a soat1-null mouse model. *Int. J. Mol. Sci.* **22**, 1583
26. Butovich, I. A., and Wilkerson, A. (2022) Dynamic changes in the gene expression patterns and lipid profiles in the developing and maturing meibomian glands. *Int. J. Mol. Sci.* **23**, 7884
27. Miyamoto, M., Sassa, T., Sawai, M., and Kihara, A. (2020) Lipid polarity gradient formed by omega-hydroxy lipids in tear film prevents dry eye disease. *Elife* **9**, e53582
28. Butovich, I. A., and Suzuki, T. (2020) Delineating a novel metabolic high triglycerides-low waxes syndrome that affects lipid homeostasis in meibomian and sebaceous glands. *Exp. Eye Res.* **199**, 108189
29. Kim, S. W., Xie, Y., Nguyen, P. Q., Bui, V. T., Huynh, K., Kang, J. S., *et al.* (2018) PPARgamma regulates meibocyte differentiation and lipid synthesis of cultured human meibomian gland epithelial cells (hMGEC). *Ocul. Surf.* **16**, 463–469
30. Kim, S. W., Rho, C. R., Kim, J., Xie, Y., Prince, R. C., Mustafa, K., *et al.* (2020) Eicosapentaenoic acid (EPA) activates PPARgamma signaling leading to cell cycle exit, lipid accumulation, and autophagy in human meibomian gland epithelial cells (hMGEC). *Ocul. Surf.* **18**, 427–437
31. Hampel, U., Kruger, M., Kunnen, C., Garreis, F., Willcox, M., and Paulsen, F. (2015) *In vitro* effects of docosahexaenoic and eicosapentaenoic acid on human meibomian gland epithelial cells. *Exp. Eye Res.* **140**, 139–148
32. Ziemanski, J. F., Wilson, L., Barnes, S., and Nichols, K. K. (2021) Triacylglycerol lipidome from human meibomian gland epithelial cells: description, response to culture conditions, and perspective on function. *Exp. Eye Res.* **207**, 108573
33. Wu, L., Belyaeva, O. V., Adams, M. K., Klyuyeva, A. V., Lee, S. A., Goggans, K. R., *et al.* (2019) Mice lacking the epidermal retinol dehydrogenases SDR16C5 and SDR16C6 display accelerated hair growth and enlarged meibomian glands. *J. Biol. Chem.* **294**, 17060–17074
34. Butovich, I. A., McMahon, A., Wojtowicz, J. C., Bhat, N., and Wilkerson, A. (2019) Effects of sex (or lack thereof) on meibogenesis in mice (Mus musculus): comparative evaluation of lipidomes and transcriptomes of male and female tarsal plates. *Ocul. Surf.* **17**, 793–808
35. Butovich, I. A. (2008) On the lipid composition of human meibum and tears: comparative analysis of nonpolar lipids. *Invest. Ophthalmol. Vis. Sci.* **49**, 3779–3789
36. Hermabessiere, L., Receveur, J., Himber, C., Mazurais, D., Huvet, A., Lagarde, F., *et al.* (2020) An Irgafos(R) 168 story: when the ubiquity of an additive prevents studying its leaching from plastics. *Sci. Total Environ.* **749**, 141651
37. Ta, C., and Bones, J. (2017) Development and validation of an ultra-performance liquid chromatography method for the determination of bis(2,4-di-tert-butylphenyl)phosphate and related extractable compounds from single-use plastic films. *J. Chromatogr. A.* **1492**, 49–54
38. Turkish, A. R., Henneberry, A. L., Cromley, D., Padamsee, M., Oelkers, P., Bazzi, H., *et al.* (2005) Identification of two novel human acyl-CoA wax alcohol acyltransferases: members of the diacylglycerol acyltransferase 2 (DGAT2) gene superfamily. *J. Biol. Chem.* **280**, 14755–14764
39. Sawai, M., Watanabe, K., Tanaka, K., Kinoshita, W., Otsuka, K., Miyamoto, M., *et al.* (2021) Diverse meibum lipids produced by Awat1 and Awat2 are important for stabilizing tear film and protecting the ocular surface. *iScience* **24**, 102478
40. Butovich, I. A., Bhat, N., and Wojtowicz, J. C. (2019) Comparative transcriptomic and lipidomic analyses of human male and female meibomian glands reveal common signature genes of meibogenesis. *Int. J. Mol. Sci.* **20**, 4539
41. Belyaeva, O. V., Lee, S. A., Adams, M. K., Chang, C., and Kedishvili, N. Y. (2012) Short chain dehydrogenase/reductase rdhe2 is a novel retinol dehydrogenase essential for frog embryonic development. *J. Biol. Chem.* **287**, 9061–9071
42. Saari, J. C., Champer, R. J., Asson-Batres, M. A., Garwin, G. G., Huang, J., Crabb, J. W., *et al.* (1995) Characterization and localization of an aldehyde dehydrogenase to amacrine cells of bovine retina. *Vis. Neurosci.* **12**, 263–272
43. Graham, C., Hodin, J., and Wistow, G. (1996) A retinaldehyde dehydrogenase as a structural protein in a mammalian eye lens. Gene recruitment of eta-crystallin. *J. Biol. Chem.* **271**, 15623–15628
44. Adams, M. K., Lee, S. A., Belyaeva, O. V., Wu, L., and Kedishvili, N. Y. (2017) Characterization of human short chain dehydrogenase/reductase SDR16C family members related to retinol dehydrogenase 10. *Chem. Biol. Interact* **276**, 88–94
45. Das, B. C., Thapa, P., Karki, R., Das, S., Mahapatra, S., Liu, T. C., *et al.* (2014) Retinoic acid signaling pathways in development and diseases. *Bioorg. Med. Chem.* **22**, 673–683
46. Hoover, F., Gundersen, T. E., Ulven, S. M., Michaille, J. J., Blanchet, S., Blomhoff, R., *et al.* (2001) Quantitative assessment of retinoid signaling pathways in the developing eye and retina of the chicken embryo. *J. Comp. Neurol.* **436**, 324–335
47. Enwright, J. F., 3rd, and Grainger, R. M. (2000) Altered retinoid signaling in the heads of small eye mouse embryos. *Dev. Biol.* **221**, 10–22
48. Yeh, T. N., and Lin, M. C. (2021) Meibomian gland contrast sensitivity and specificity in the diagnosis of lipid-deficient dry eye: a pilot study. *Optom. Vis. Sci.* **98**, 121–126
49. Butovich, I. A., Lu, H., McMahon, A., and Eule, J. C. (2012) Toward an animal model of the human tear film: biochemical comparison of the mouse, canine, rabbit, and human meibomian lipidomes. *Invest. Ophthalmol. Vis. Sci.* **53**, 6881–6896